INVESTIGATION OF WING STALL DELAY EFFECT DUE TO AN UNDULATING LEADING EDGE: AN LES STUDY

Alex Skillen

Computational Fluid Dynamics group,
Modelling and Simulation Centre,
School of MACE,
The University of Manchester, UK
alex.skillen@manchester.ac.uk

Alistair Revell

Computational Fluid Dynamics group,
Modelling and Simulation Centre,
School of MACE,
The University of Manchester, UK
alistair.revell@manchester.ac.uk

Julien Favier

Laboratoire de Mécanique, Modélisation et Procédés Propres (M2P2),
Aix-Marseille Université,
UMR7340 CNRS, 13451 Marseille, France
Julien.Favier@univ-amu.fr

Alfredo Pinelli

School of Engineering and Mathematical Science,
City University London.
a.pinelli@ciemat.es

Ugo Piomelli

Dept. of Mechanical and Materials Engineering,
Queen's University,
Kingston (Ontario) K7L 3N6, Canada.
ugo@me.queensu.ca

Abstract

We present LES simulations of the flow over a wing with sinusoidal leading edge undulations. The undulations act as a passive flow control device, offering superior post-stall aerodynamic performance relative to the unmodified wing with the same mean chord. The baseline case of a regular wing is also presented for comparison. In all cases the Reynolds number based on bulk velocity and mean chord is equal to $120,000$, and the angle of attack is set to $20°$.

The study explores the details of the flow physics and the mechanisms by which the post-stall aerodynamic benefit is gained. For the particular set of geometrical and aerodynamic parameters considered, a hitherto unreported physical mechanism by which the undulation offers their benefit is observed. This increased understanding of the flow physics for the current configuration is an important step towards a more general understanding and the incorporation of the technology into practical designs. Potential applications include vertical axis wind turbines, unmanned air vehicles, helicopter blades, and canard surfaces; the present Reynolds number is of particular relevance to the first two of these applications.

Introduction

Inspired by the high maneuverability of the humpback whale, there has been a surge in interest in the mammal's hydrodynamic performance, with a view towards capitalising on findings in the field of biomimetics. A key contributing factor to this high maneuverability is the form of the pectoral flippers; specifically the presence of protuberances
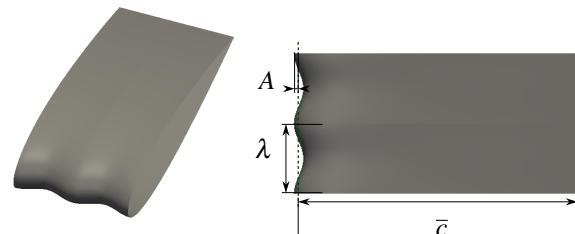

Figure 1.   Geometry considered

(or undulations) along the leading edge, which act as a passive flow control device delaying separation.

Several attempts have been made to elucidate the physical mechanisms by which the undulations offer their benefit. Fish *et al.* (2011) present a morphological study and suggest the undulations act as vortex generators, re-energising the boundary layer. They also suggest the undulations may increase the effective span of a finite wing by diminishing the spanwise flow component, thereby reducing the strength of the wing-tip vortex. Stanway (2008) performed PIV measurements around a finite wing with protuberances. Pairs of vortical structures were observed emanating from each protuberance. Stanway suggests a physical mechanism similar to that of a delta wing, whereby chord-wise vortices generate lift.

Favier *et al.* (2012) conducted numerical simulations of an undulating geometry at $Re = 800$ and an angle of attack of $20°$. A parametric study was performed on the undulations, covering a range of wavelengths and amplitudes.
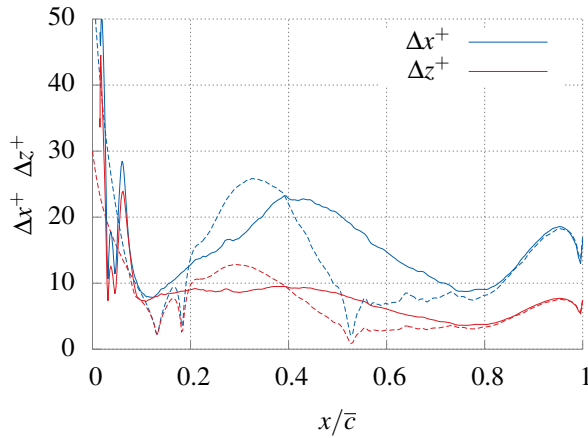
Figure 2. Grid spacing in wall units. Dashed; behind chord maxima: Solid; behind chord minima.

While the authors observed a peak drag reduction of 35%, the lift was also reduced relative to the baseline unmodified case for all configurations. This inauspicious result is likely to be a consequence of the low flow Reynolds number considered (several orders of magnitude lower than that observed in nature, and lower than that required for transition to turbulence). In the study, a Kelvin-Helmholtz-like instability was identified, driven by the spanwise modulation of the streamwise velocity component, induced by the undulations. It was reasoned that this instability acts to produce rolls of vorticity emanating from the undulation site. The rolls, initially vertical, are then tilted into the streamwise direction as they are advected by the flow. The vortices decrease drag by acting on boundary-layer separation and promoting attachment.

Miklosovic *et al.* (2007) performed wind tunnel measurements on both infinite and finite wings with an undulating leading edge. They found a significant performance decrease for the infinite wing relative to their finite span model, leading to the suggestion that the protuberances gained their benefit via interaction with the wing tip vortices, and that the benefit would be best realised in the case of a finite wing. However, it must be noted that in their study, the operating Reynolds number for the infinite case was less than half that of the finite span. Stanway (2008) showed a strong sensitivity of the performance enhance-
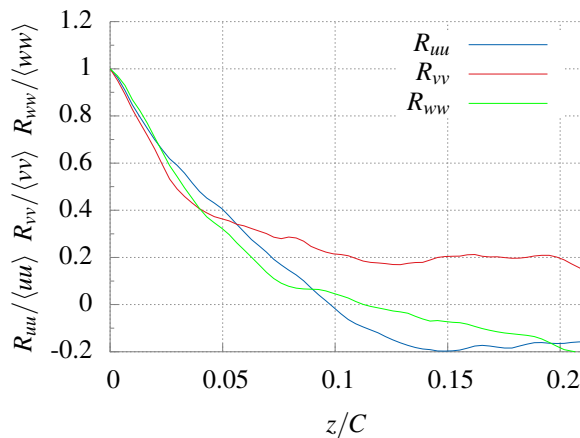

Figure 3. The two-point correlation in shear layer.
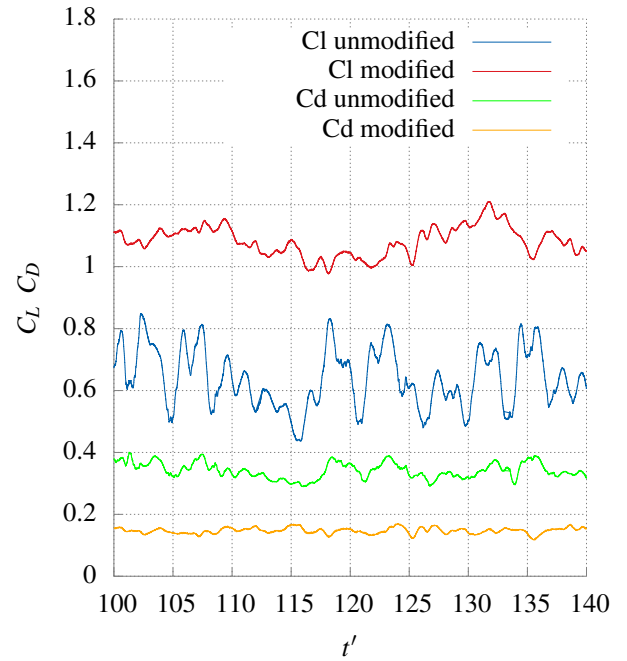

Figure 4. Instantaneous lift and drag coefficients for both modified and unmodified geometries.

ment to the flow Reynolds number, thereby casting doubt over the proposed significance of the wing tip vortices.

Hansen *et al.* (2011) performed a series wind tunnel measurements over sinusoidal undulating geometries, covering a wide range of wavelengths and amplitudes. The study also considered both finite and infinite wing configurations, all at $Re = 120,000$. The authors show that both the finite and infinite configurations offered a similar performance benefit, further indicating that the wing tip effect is not as significant as originally thought.

While some insight has been gained into the principal flow mechanisms, a detailed flow physics investigation has not been provided thus far. Specifically, while the performance benefit has been quantified in terms of the integral quantities for a range of different wavelengths and undulation amplitudes (Hansen *et al.*, 2011), the effect of these parameters on the flow physics is unclear. Moreover, the effect of Reynolds number on the flow physics has not been explored in any great detail. While it is generally accepted that the undulations induce a vortex system, there is no general consensus over the mechanisms by which this vortex is driven; indeed it may be the case that fundamentally different mechanisms are involved for different geometrical configurations and flow Reynolds numbers.

In the present study, we outline LES calculations of the flow over a wing with sinusoidal leading edge undulations. The flow Reynolds number based on mean chord length and bulk velocity is $120,000$, and the incidence angle is set to $20°$. It will be shown that under these conditions, the main physical mechanism involved originates from a secondary flow induced by the undulations. This secondary flow acts to transport low momentum fluid from behind the chord peak, thereby re-energising the boundary layer, which reduces the size of the separated region. The reduction in the size of the separated region presents a favourable effective aerodynamic form (relative to the baseline case of a wing without undulations at the same angle of attack and flow
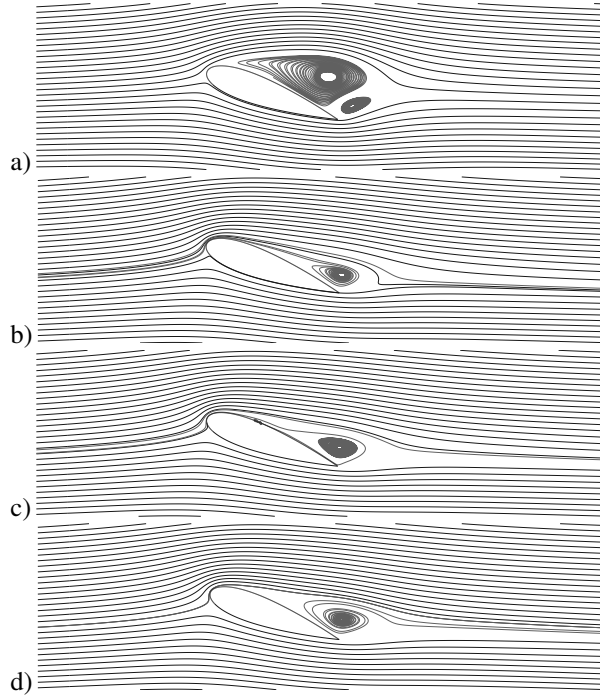
Figure 5. Time averaged streamlines in xy-plane. a) unmodified geometry. b) chord maxima. c) mean chord. d) chord minima

conditions), thereby significantly improving aerodynamic performance.

Numerical approach

The filtered incompressible Navier Stokes equations govern the flow development;

$$
\frac{\partial \overline{u}_i}{\partial t} + \frac{\partial}{\partial x_j} \left(\overline{u}_i \overline{u}_j \right) =
$$
$$
\frac{\partial}{\partial x_j} \left[-\overline{p} \delta_{ij} + \nu \left(\frac{\partial \overline{u}_i}{\partial x_j} + \frac{\partial \overline{u}_j}{\partial x_i} \right) - \tau_{ij} \right] \quad (1)
$$
$$
\frac{\partial \overline{u}_i}{\partial x_i} = 0
$$

where an overbar denotes a filtered field, and τ_{ij} is the residual stress tensor. The filtering operation is performed implicitly by the mesh.

Equations 1 are closed via an eddy viscosity model;

$$
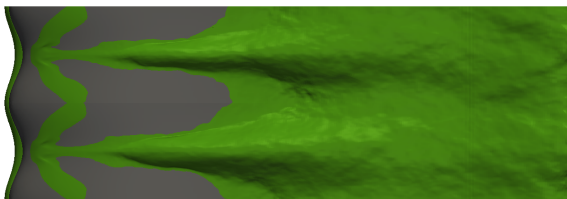\tau_{ij} = -2c_s \Delta^2 \left| \overline{S} \right| \overline{S}_{ij} \quad (2)
$$

Figure 6. Iso-surface of zero streamwise time-average velocity. Plan view.

where $\overline{S}_{ij}$ is the resolved strain rate tensor, $|\overline{S}| = \sqrt{2\overline{S}_{ij}\overline{S}_{ij}}$, and Δ is the local filter width, taken as $V^{1/3}$ (where V is the cell volume). The model constant $c_s(\mathbf{x}, t)$ is set according to the Germano-Lilly dynamic procedure (Germano *et al.*, 1991; Lilly, 1992).

The governing equations are discretised via the Finite volume method. We use a central scheme for the interpolation of face values in convective and viscous flux terms. For temporal discretisation, a second order implicit scheme is used. A temporally varying time-step size is used, set to yield a maximum global Courant number of unity. Pressure velocity coupling is achieved via the PISO algorithm (Ferziger & Perić, 1996).

The discretised equations are solved iteratively using the OpenFOAM package until first and second order statistics are fully converged. Statistics are gathered over 400 dimensionless time units (defined as $t' \equiv Ut/\overline{c}$, where U is the bulk velocity, t and t' are the physical and dimensionless times respectively, and $\overline{c}$ is the mean chord). The initial transient phase does not contribute towards the statistics.

Geometry and mesh

Figure 1 shows the undulating geometry of the present study. A NACA 0021 wing section is employed and is set at an angle of attack of $20°$; a post-stall condition. The chord length for the undulating cases varies as:

$$
c(z) = A \cos\left(\frac{2\pi z}{\lambda} \right) + \overline{c} \quad (3)
$$

where A is the amplitude of the undulation, λ is the wavelength of the undulation, and z is the spanwise ordinate. For the undulating case considered herein, we use $A = 0.015\overline{c}$ and $\lambda = 0.21\overline{c}$. The baseline unmodified NACA 0021 profile is also computed for comparison.

The extents of the computational domain reach $10\overline{c}$ upstream of the leading edge, and $15\overline{c}$ downstream of the trailing edge. Lateral boundaries are placed $15\overline{c}$ from the wing. The extent of the domain in the spanwise direction is set at $0.42\overline{c}$ for both the unmodified and undulating cases, corresponding to two wavelengths of the undulation.

Meshes comprising around 3.5×10^7 cells have been used, with around $150,000$ cells in each xy-plane. All meshes are of block-structured hexahedral topology, with a 'C-shape' grid being wrapped around the wing. The same mesh density in the xy-plane is used for all cases, with the mesh being smoothly adjusted to conform to the contour of the geometry at the undulation site. Near wall cells are placed at $y^+ < 1$ in all cases. Between 5 and 10 computational cells occupy the near-wall region $y^+ < 10$, depending on the local flow conditions. Figure 2 shows the grid spacing in terms of wall units for the modified case behind the chord maxima as well as the chord minima. Grid sensitivity tests have been conducted with cell counts around 50% lower than that presented herein. No fundamental differences to the physical mechanisms involved were observed at the reduced cell count (though the quantitative results for the integral quantities did differ by a few per cent).

To asses whether or not the spanwise extent is sufficient to capture the requisite turbulent physics, we compute the two-point correlation (defined as $R_{ij}(\mathbf{x}, \mathbf{r}) \equiv \langle u_i(\mathbf{x})u_j(\mathbf{x} + \mathbf{r}) \rangle$) between a point at $\mathbf{x}$, and a second point displaced by $\mathbf{r}$
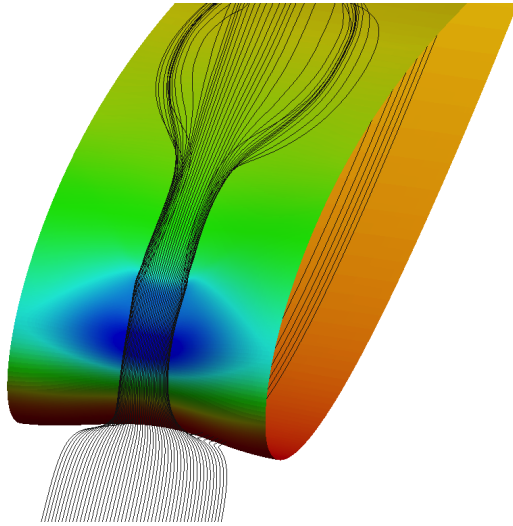
Figure 7. Time averaged streamlines showing deflection on oncoming flow at the leading edge region. Half span shown for clarity. Colour pressure (blue to red).

from **x** (where **r** is a vector pointing in the spanwise direction). Several locations **x** in the separated shear layer and recirculation region have been considered; the most strongly correlated case is presented in Figure 3. While it can be seen that the span is insufficient to reduce the two-point correlation to zero by the edge of the domain at all locations **x**, the correlation was deemed sufficiently low to have confidence that the correct underlying physics is captured. Indeed, tests
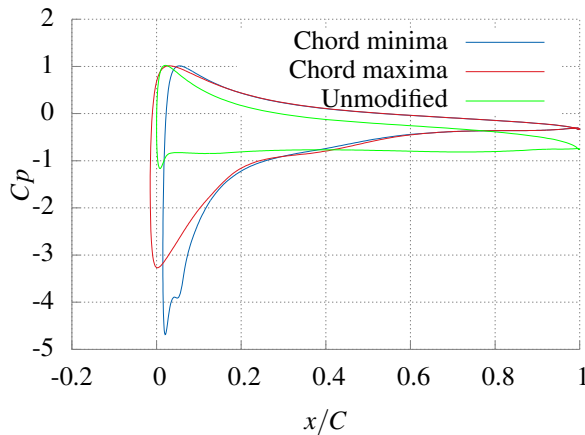

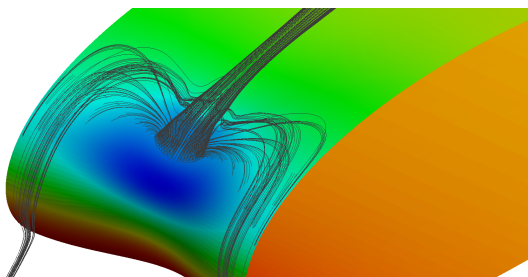Figure 8. Surface pressure coefficient.

Figure 9. Time averaged streamlines showing secondary flow feature. Half span shown for clarity. Colour pressure (blue to red).

Table 1. Mean lift and drag coefficients

	$\langle Cl \rangle$	$\langle Cd \rangle$
Unmodified	0.75	0.32
Modified	1.02	0.24

with a reduced spanwise extent (not presented) revealed no differences to the primary physical mechanisms at play.

Boundary conditions

A uniform velocity is applied at the inlet, with zero free-stream turbulence. Lateral boundaries are modelled as slip walls. At the outlet, a zero pressure condition is employed, while periodicity is applied in the spanwise direction. The wing surface is modelled as a non-slip wall with zero surface-velocity and a zero gradient condition in the wall-normal direction for the surface pressure. No special treatment is required at the wall since the grid is sufficiently fine to resolve fully the fluid boundary layer. Moreover, the dynamic sub-grid model employed is known to give correct asymptotic behaviour on approaching a solid surface without the need for damping functions.

It is expected that there will be a sensitivity of the flow to the incoming turbulence levels. However, such an investigation is left as future work.

Results

Figure 4 shows the time history of lift and drag coefficient for both the undulating and baseline cases. Table 1 shows the time-averaged force coefficients. It can be seen that the undulating geometry yields a 36% increase in mean lift, and a 25% decrease in mean drag. Moreover, is is clear that the undulating modifications act to remove much of the unsteadiness from the flow, since the variance in the force coefficients is reduced. This is important for applications where noise suppression is desired, such as in the design of fans.

Figure 5 provides streamlines of mean velocity in the *xy*-plane at the peak chord, mid chord and minimum chord for the undulating geometry. The unmodified case is also presented for comparison. It is apparent from the figure that the size of the recirculation region for the undulating case is dramatically reduced at all spanwise locations, relative to the unmodified geometry. This is also apparent from Figure 6, which shows an iso-surface of zero streamwise velocity component. The reduced size of the separation region explains the improved aerodynamic performance.

The observed mechanism by which the undulations reduce the size of the separated region is elucidated as follows. Oncoming flow is deflected by the leading-edge geometry such that the bulk of the flow is directed behind the chord minima (see Figure 7). This leads to a strong acceleration behind the minima, and consequently forms an enhanced suction peak (relative to the region behind the maxima). Figure 8 demonstrates this via plots of the pressure coefficient behind both the chord maxima and chord minima. The unmodified case is also plotted for comparison. This spanwise pressure gradient drives the development of a secondary flow, whose influence appears key to attaining the intended aerodynamic benefit.

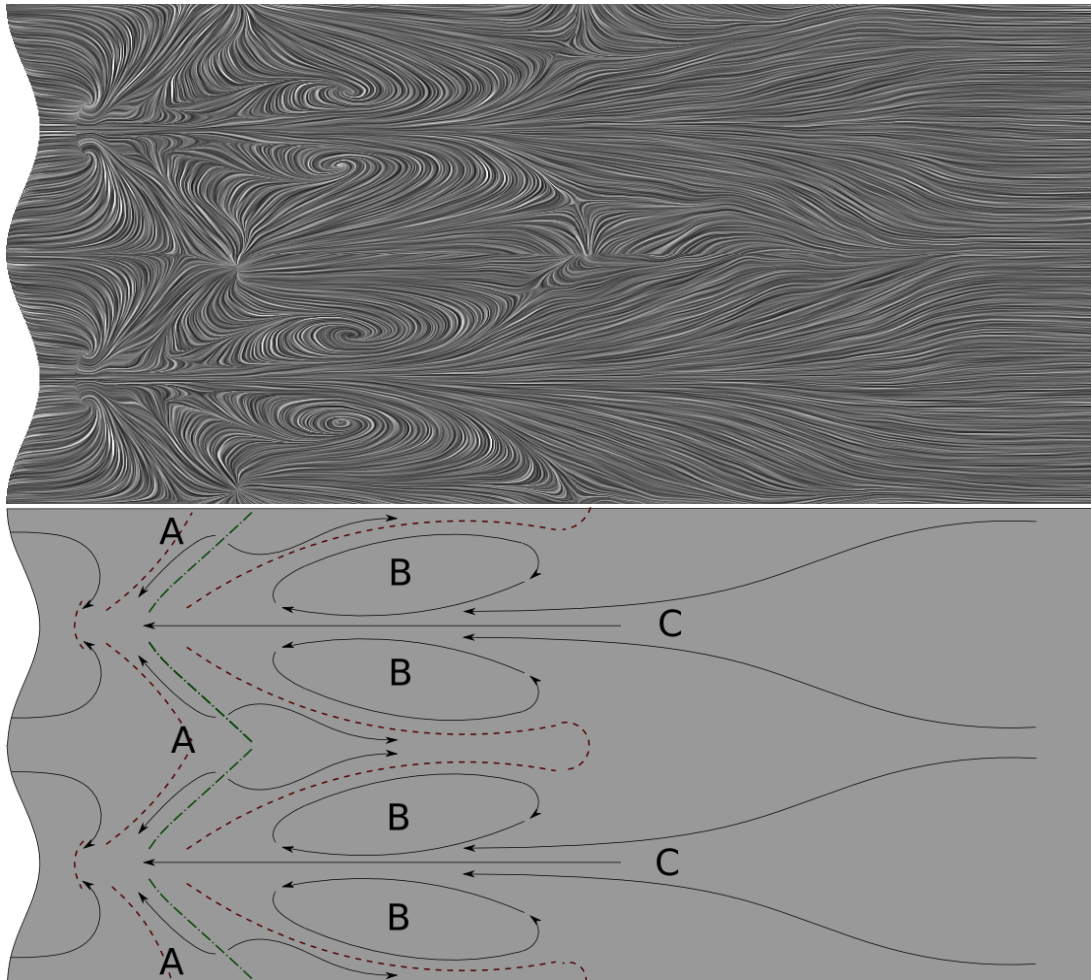The effect of the suction peak downstream of the chord

Figure 10.   Wall shear stress visualised with the line integral convolution technique (Cabral & Leedom, 1993) (above). Sketch showing flow direction (arrows), separation lines (red dashed), and reattachment lines (green dot-dash) (below).

minima, combined with the reduced local chord length, leads to a large adverse pressure gradient, and ultimately to flow separation a short distance downstream of the leading edge. The enhanced suction behind the minima draws low inertia boundary-layer fluid from behind the chord maxima to behind the minima, as can be seen from Figure 9. Significantly, the low-inertia boundary-layer fluid that is transported away by this secondary flow is replaced by high momentum fluid, drawn from above, thereby delaying separation behind each undulation peak and reducing the size of the recirculation region. This is thought to be the primary mechanism involved.

It is observed that the adverse pressure gradient induces a laminar separation across the entire span, which is progressively delayed on approach of the chord peak (see Figure 10, label A). Transition is clearly observed to occur in the separated shear layer due to the amplification of perturbations via the Kelvin-Helmholtz mechanism (see Figure 11). Subsequent to this, momentum transfer due to turbulent mixing quickly reattaches the shear layer, at which point the fluid bifurcates into a laminar separation bubble and a newly energised boundary layer upstream and downstream of the reattachment point respectively.

It can be seen in Figure 10 that a large vortex system is generated, labelled B. This vortex is driven primarily by viscous shear interaction, and hence extracts momentum from the streamwise component of the flow. This feature acts to transport momentum from behind the chord maxima to behind the minima, thereby regulating the size of the recirculation zone across the span. It should be noted, however, that the energy contained in this vortex system is relatively low, and hence it should have a comparatively small effect on the mean flow. Low inertia fluid in the recirculation zone is entrained into this vortex, as can be seen in the figure (label C).

In addition to the transport of momentum by the secondary flow, the nature of the turbulent fluctuations also appears to aid preferential flow attachment behind the chord peak. Hairpin structures can be clearly observed in the separated shear layer, immediately downstream of the initial laminar separation line associated with the secondary flow (see Figure 11). The direction of these hairpin vortices is such that, on average, the streamwise flow component is augmented in the region behind the chord maxima, with a resulting attenuation of flow behind the minima. This intensifies the effect already described and promotes attachment behind the maxima.

Conclusion

Wall-resolved LES simulations are presented for the flow over a NACA 0021 wing with leading edge undulations. An undulation amplitude of 1.5% chord and a wavelength of 21% chord is considered. For this case, a 36%
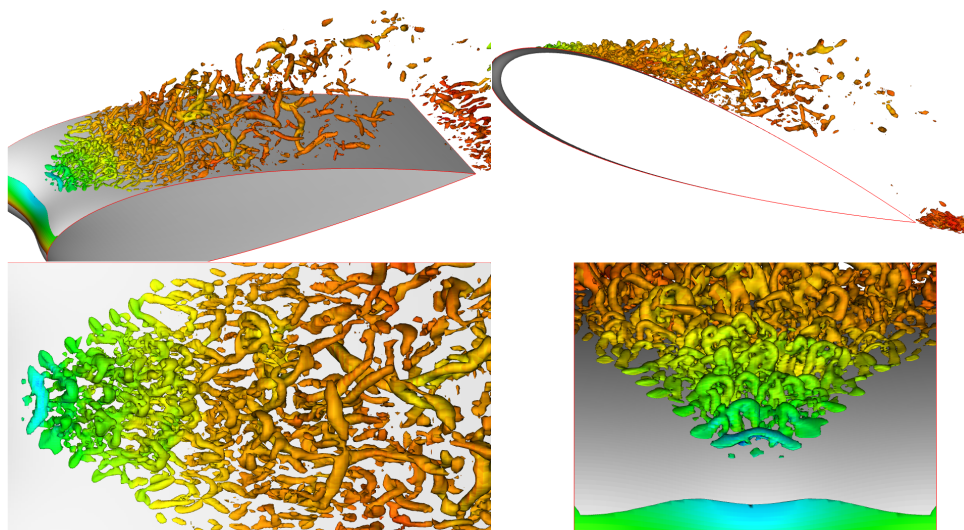
Figure 11. Iso-surfaces of Q=200. Colour pressure (blue to red).

increase in mean lift and a 25% decrease in mean drag is observed. It is observed that this performance enhancement arises by virtue of the fact that the size of the separated zone is significantly reduced (relative to that of the standard NACA 0021 wing), thereby yielding a superior effective aerodynamic shape.

The mechanisms by which the size of the separation zone is reduced are explored. It is shown that the undulations induce a strong spanwise pressure gradient due to the fact that the bulk of the oncoming flow is redirected behind the chord minima. This spanwise pressure gradient induces a secondary flow; low inertia boundary-layer fluid from behind the peak chord is transported in the spanwise direction toward the suction peak. High momentum fluid from above replaces the boundary-layer fluid, thereby re-energising the boundary layer behind the chord maxima, delaying separation. While it is thought that this is the primary mechanism, the nature of the turbulent fluctuations also plays a role in promoting attachment since hairpin vortices augment the streamwise flow behind the chord maxima, thereby delaying separation.

This proposed mechanism by which the undulations offer their aerodynamic benefit is significantly different to the speculative ideas proposed in e.g. (Fish *et al.*, 2011; Stanway, 2008). It is also significantly different to that observed at low Reynolds numbers (Favier *et al.*, 2012), though there may be an element of the Kelvin-Helmholtz-driven mechanism contributing here. Further simulations (not presented) show that the primary mechanism (i.e. the transport of momentum by a secondary flow) is consistent over a range of geometrical parameters at the Reynolds number considered herein, though the details of the downstream physics and magnitude of the benefit vary. Future work will explore the parameter space further.

Acknowledgement

REFERENCES

Cabral, Brian & Leedom, Leith Casey 1993 Imaging vector fields using line integral convolution. In *Proceedings of the 20th annual conference on Computer graphics and interactive techniques*, pp. 263–270. ACM.

Favier, Julien, Pinelli, Alfredo & Piomelli, Ugo 2012 Control of the separated flow around an airfoil using a wavy leading edge inspired by humpback whale flippers. *Comptes Rendus Mécanique* **340** (1-2), 107–114.

Ferziger, Joel H & Perić, Milovan 1996 *Computational methods for fluid dynamics*, , vol. 3. Springer Berlin.

Fish, Frank E, Weber, Paul W, Murray, Mark M & Howle, Laurens E 2011 The tubercles on humpback whales' flippers: application of bio-inspired technology. *Integrative and comparative biology* **51** (1), 203–13.

Germano, Massimo, Piomelli, Ugo, Moin, Parviz & Cabot, William H 1991 A dynamic subgrid-scale eddy viscosity model. *Physics of Fluids A: Fluid Dynamics* **3**, 1760.

Hansen, K L, Kelso, R M & Dally, B B 2011 Performance Variations of Leading-Edge Tubercles for Distinct Airfoil Profiles. *AIAA Journal* **49** (1), 185–194.

Lilly, DK 1992 A proposed modification of the germano subgrid-scale closure method. *Physics of Fluids A: Fluid Dynamics* **4**, 633.

Miklosovic, David S., Murray, Mark M. & Howle, Laurens E. 2007 Experimental Evaluation of Sinusoidal Leading Edges. *Journal of Aircraft* **44** (4), 1404–1408.

Stanway, Michael Jordan 2008 Hydrodynamic effects of leading-edge tubercles on control surfaces and in flapping foil propulsion. PhD thesis, MIT.